Journal of Green Energy Research and Innovation

A Cutting-Edge Reliability Assessment of MPPT-Driven Photovoltaic Systems Enhanced by Recursive Least Squares Adaptive Identification

Peyman Bayat, Pezhman Bayat

Highlights

- **RLS-driven dynamic parameter identification for MPPT reliability assessment.**
- **Hierarchical MPPT categorization framework for reliability benchmarking.**
- **Irradiation set-point isolation methodology.**
- **Direct correlation between MPPT dynamics and grid reliability.**

Graphical Abstract

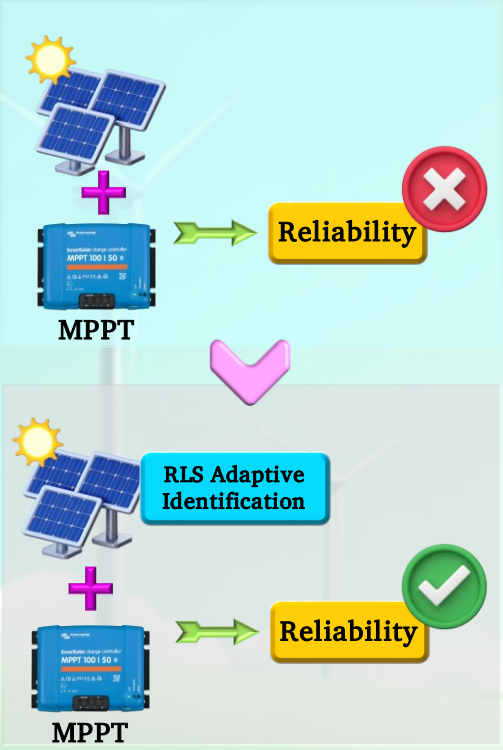

Use your device to scan and read the article online

Citation

P. Bayat, and P. Bayat," A Cutting-Edge Reliability Assessment of MPPT-Driven Photovoltaic Systems Enhanced by Recursive Least Squares Adaptive Identification," *Journal of Green Energy Research and Innovation*, vol. 2, no. 3, pp. 72-93, 2025.

https://doi.org/10.61882/jgeri.2.3.72

Journal of Green Energy Research and Innovation 2.3 (2025) 72-93

Online ISSN: 3041-9018

Journal of Green Energy Research and Innovation

Journal Homepage: www.jgeri.araku.ac.ir

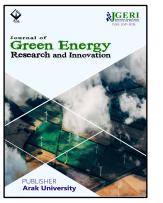

A Cutting-Edge Reliability Assessment of MPPT-Driven Photovoltaic Systems Enhanced by Recursive Least Squares Adaptive Identification

Peyman Bayat [*] , Pezhman Bayat

Department of Electrical Engineering, Hamedan University of Technology, Hamedan, Iran.

ARTICLE INFO

Keywords:
Solar energy
Reliability metrics,
System identifications,
Maximum power point tracking.

Article History:
Received: 12 March 2025;
Revised: 04 May 2025;
Accepted: 12 May 2025.

Article type:
Research Article

[*] ***Corresponding author***
E-mail address
peyman.bayat@hut.ac.ir (P.Bayat)

ABSTRACT

Solar energy has become an important global energy research topic, recognized for its potential to address sustainability challenges. While photovoltaic (PV) technology offers clean energy generation, its broader adoption is constrained by limitations such as suboptimal conversion efficiency and high perceived initial costs. This study explores the influence of various maximum power point tracking (MPPT) methods on the reliable performance of PV systems that operate in network-connected mode. It investigates how these power optimization strategies impact overall operational reliability, emphasizing the role of MPPT in achieving stable and efficient grid integration. By categorizing MPPT techniques into offline, online, and hybrid groups, the research assesses their impact on reliability metrics within a standardized distribution network. Using the recursive least squares (RLS) method, localized solar cell parameters are dynamically estimated under different MPPT configurations. To isolate the effects of methodologies, irradiation fluctuations are treated as controlled set-point adjustments. Simulation results conducted with MATLAB/Simulink reveal statistically significant correlations between MPPT selection and system reliability, providing actionable insights for enhancing PV grid integration.

1. Introduction

The intensifying global energy crisis, together with the worsening impacts of climate change, has driven a remarkable increase in the adoption of renewable energy and sustainable fuel technologies. This shift represents a critical departure from our prolonged reliance on finite fossil fuel resources, while actively aiming to mitigate additional environmental damage. To explain further, with energy supplies becoming scarcer and environmental challenges mounting, societies worldwide are driven to seek cleaner and more sustainable energy solutions [1]. This increasing focus on renewable energy signifies not only an essential shift towards sustainable energy sources but also highlights the pressing need to safeguard our planet against the harmful consequences of excessive fossil fuel usage. Renewable energy sources, including wind, ocean waves, tidal forces, solar radiation, biomass, biofuels, and geothermal heat, act as potential energies for electricity generation. The conversion of these resources into electrical energy occurs through both direct and indirect methods, depending on the technology employed. For instance, solar thermal power plants utilize concentrated solar energy to heat fluids, which drive turbines to generate electricity indirectly. In contrast, photovoltaic (PV) cells bypass intermediate steps by directly converting sunlight into direct current (DC) electricity through the photovoltaic effect, a quantum mechanical phenomenon that liberates electrons when photons strike semiconductor materials [2]. The integration of renewable energy into modern infrastructure involves two primary pathways: grid-connected systems, where electricity is fed into centralized power networks, and off-grid applications, which provide decentralized energy access to remote or underserved regions. This dual approach underscores the adaptability of renewable technologies to diverse energy needs [1,2]. One objective of advancing renewable energy systems is reliability modeling, a technique aimed at identifying unforeseen outages, forecasting potential failures, and quantifying performance metrics such as failure rates and mean time to failure (MTTF) [2].

By analyzing potential faults and component failures, engineers can refine system designs to meet strict reliability standards. To achieve this, methodologies like failure modes and effects analysis (FMEA) systematically list failure scenarios and their impacts, while fault tree analysis (FTA) illustrates the relationships between component failures and system-wide malfunctions [2,3]. Markov analysis (MA) employs probabilistic models to forecast system behavior over time, and probabilistic risk assessment (PRA) quantifies the probability and consequences of adverse events [4]. Reliability block diagrams (RBD) complement these tools by visually representing the interdependencies of system components, enabling engineers to accurately identify critical failure points [4-7].

Despite these methodologies, developing renewable energy systems with reliability comparable to conventional power grids presents significant challenges. A significant challenge lies in the inherent instability of renewable energy sources, especially solar PV systems. These systems exhibit output fluctuations due to their dependence on weather conditions, such as cloud cover, temperature shifts, and variations in solar irradiation. For example, abrupt weather changes can cause rapid swings in solar irradiance, leading to sudden spikes or drops in power generation. This variability complicates grid stability, as traditional energy storage solutions like batteries often lack the capacity or response time to buffer such transient power changes effectively [8].

To address these challenges, researchers have focused on fine-tuning the maximum power point (MPP) of photovoltaic modules. The MPP is the specific operating condition where a PV system produces its highest possible power output given the current environmental factors. Advanced maximum power point tracking (MPPT) techniques are essential for dynamically adjusting system parameters to maintain operation at or near the MPP [8]. These techniques are broadly categorized into three groups:

- **Offline Methods:** Offline techniques depend basically on detailed solar cell models to estimate the MPP. In these approaches, the characteristics of the PV module, such as its voltage and current behavior under varying irradiance and temperature, are known in advance, and specific model parameters are used to compute the optimum operating point. Commonly, methods such as the short circuit current (SCC) approach, open circuit voltage (OCV) approach, and artificial intelligence-based methods such as artificial neural networks (ANN) are suggested as popular methods [8]. In practical implementations, these methods aim to identify essential electrical parameters, particularly the V_{OC}, which denotes the voltage in an open-circuit condition, and the I_{SC}, which signifies the current in a short-circuit condition. These approaches achieve their goals by employing two primary strategies; one approach involves actively forcing the system into an open or short circuit state so that the parameter can be measured directly. Alternatively, the values of V_{OC} or I_{SC} can be estimated indirectly by using temperature and irradiance measurements to calculate these parameters. The accuracy of these indirect calculations depends on the accuracy of the characteristic data supplied by the manufacturer; however, an advantage of this computed approach is that it avoids the power interruption that direct measurements may require. Once V_{OC} or I_{SC} is determined, these values are transformed into control signals that continuously direct the PV system toward its MPP. Provided that environmental conditions remain stable, these signals do not change, maintaining a constant operating point.

- **Online Methods:** Contrary to offline strategies, online methods do not require a prior model of the solar cell. Instead, they dynamically track the MPP using real-time measurements of PV voltage and current. These methods introduce a small, systematic perturbation, be it in voltage, current, or duty cycle, to induce a variation in the output power. By analyzing how the output power responds to each perturbation, the system determines whether to increase or decrease the control signal, thereby progressively guiding the operating point toward the MPP. This real-time adjustment leads to a continuously changing control signal and, consequently, introduces slight oscillations about the optimum point. Techniques such as perturbation and observation method (P&O), extremum seeking control method (ESC), and incremental conductance method (IncCond) fall under this category [9,10]. One clear benefit of the P&O approach is that it does not rely on detailed knowledge of the panel's specific characteristics. However, when conditions change rapidly (as under fluctuating irradiance), the P&O method often faces challenges due to the inherent delays in sampling and adjustments, leading researchers to develop numerous improvements to enhance its performance in dynamic conditions [10].

- **Hybrid Methods:** Hybrid methods merge the strengths of both offline and online approaches to achieve a more robust MPPT strategy. Typically, these methods are executed in three phases. First, the system establishes an initial operating point based on offline computations, using predetermined parameters to set a system MPP. Next, this initial value is refined through iterative online fine-tuning loops that continuously adjust the control signal as real-time measurements are acquired. For example, one study [11] integrates the system's impedance and efficiency factors by coupling a DC-DC boost converter with a battery load, which serves as a substitute for the standard load. In this particular hybrid implementation, the control process is structured into two loops: the first loop estimates the MPP from the open circuit voltage under steady temperature conditions, and the second loop employs the P&O method to fine-tune the positioning of the MPP by determining the accurate maximum output power. To ensure that the system responds quickly to changes while also maintaining stable performance, the amplitude and frequency of the perturbations in the online loop are minimized. Graphically, as depicted in Figure 1, the overall control signal is constructed from an offline component that sets the initial target and an online component that continuously refines the target.

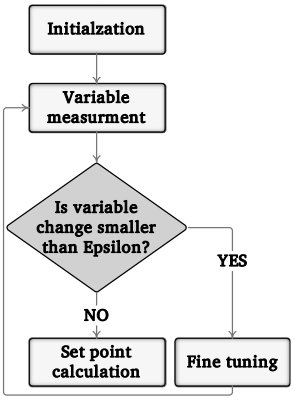

Figure 1. General flowchart used in hybrid MPPT methods.

This study thoroughly examines the impact of various MPPT methods on the reliability of PV systems operating in grid-connected modes and classifies MPPT methods into three main categories to encompass their diverse mechanisms and operational complexities, e.g., offline, online, and hybrid approaches. For a comprehensive analysis, simulations were conducted using three distinct offline methods, which include ANN, OCV, and SCC, alongside two online techniques, P&O and ESC, as well as two hybrid configurations (labeled as hybrid [11] and hybrid [12]). Each of these techniques represents a unique way of tracking the MPP, and by simulating them, the study can compare their performance in a consistent framework. A critical component of the analysis is the dynamic identification of PV system parameters. To achieve this, the RLS algorithm is employed, ensuring that the local PV system model is accurately updated under the influence of each MPPT approach. This allows for an accurate assessment of the PV system's performance across different tracking strategies, capturing real-time variations in operating conditions. To isolate the impact of various MPPT techniques, variations in solar irradiation, an inherently fluctuating factor, are modeled as changes in the set point. This approach ensures that any shifts in the operating conditions, due to irradiance variability, are directly incorporated into the analysis, allowing each MPPT technique to be evaluated on a level playing field. The simulations, carried out within the MATLAB/Simulink environment, yielded clear results that demonstrate direct correlations between the MPPT technique employed and the overall system reliability. These findings highlight the main influence of MPPT strategies on the performance and reliability of PV systems operating in grid-connected mode.

1.1. Innovative Contributions

To highlight and discuss the innovative contributions of this paper, the key points can be summarized as follows**:**

- **RLS-driven dynamic parameter identification for MPPT reliability assessment:** This research introduces the innovative application of the RLS algorithm in combination with varying MPPT techniques to dynamically identify and model localized PV system parameters (e.g., series resistance, shunt impedance). By enabling real-time adaptation of reliability models to changing environmental and operational conditions, it bridges the gap between theoretical MPPT performance and practical system robustness.
- **Hierarchical MPPT categorization framework for reliability benchmarking:** The paper presents an organized classification system for MPPT methods, categorized into offline, online, and hybrid approaches, and benchmarks their reliability impacts through seven distinct algorithms, including recent hybrid techniques. This represents the first comparative analysis connecting MPPT categories to reliability metrics, offering practical guidelines for selecting optimal MPPT strategies based on grid resilience needs.
- **Irradiation set-point isolation methodology:** This innovative approach treats irradiation variations as controlled set-point adjustments rather than stochastic disturbances, effectively isolating the influence of MPPT dynamics on system reliability. By eliminating confounding variables, the methodology precisely attributes reliability fluctuations to specific MPPT behaviors, such as the fluctuations characteristic of P&O methods compared to the more stable transitions achieved by hybrid approaches.
- **Direct correlation between MPPT dynamics and grid reliability:** This study provides conclusive results demonstrating that hybrid MPPT methods (e.g., [11], [12]) reduce grid-side total harmonic distortion compared to conventional online methods like P&O. However, offline methods such as ANN and OCV are shown to compromise transient stability during rapid irradiation shifts. Quantifiable metrics are provided to inform the design of fail-safe PV systems for critical grid applications.

1.2. Paper Organization

This research is presented through the following step-by-step structure to achieve its objectives. Section 2 establishes the context for the present research by describing the architecture of the grid-connected PV system under study. It analyzes the operational principles of selected MPPT algorithms and develops mathematical models for critical system components. A dedicated subsection examines PV system parameter identification, comparing how different MPPT strategies affect the accuracy of these estimations. For example, it evaluates the influence of voltage ripple patterns in perturbative MPPT methods on parameter estimation under dynamic

weather conditions. Section 3 presents a detailed comparative analysis of simulation results, assessing the impact of various MPPT techniques, from conventional P&O to hybrid ANN-based methods, on long-term system reliability metrics. These metrics include component degradation rates, inverter stress profiles, and grid synchronization stability during irradiance transients. The section also employs quantitative benchmarking to link MPPT-induced electrical oscillations with failure probabilities. Section 4 extends the analysis to explore distribution network impacts, investigating how MPPT-driven power fluctuations affect grid infrastructure. This includes harmonic distortion analysis, voltage regulation challenges during partial shading events, and protection coordination requirements for varying levels of PV penetration. Case studies are included to demonstrate how adaptive MPPT configurations can mitigate cascading reliability risks in weak grid conditions. Section 5 integrates empirical and theoretical findings into actionable insights, highlighting the relationship between MPPT algorithm complexity and measurable improvements in both energy yield and system lifespan. The conclusion proposes updated cost-benefit paradigms that reflect the reliability gains associated with advanced MPPT strategies, offering new perspectives on PV system affordability based on lifecycle performance.

2. System Under Investigation

To thoroughly analyze the influence of MPPT techniques on the reliability of PV systems operating in grid-connected mode, it is essential to create a robust and detailed PV model that appropriately represents the complex interdependencies among key system parameters, including solar irradiation, temperature, and electrical properties. This detailed model serves as the foundation for understanding how fluctuations in these factors influence the overall performance and stability of the system. The system model under investigation, exemplifying an integrated PV power system, is depicted in Figure 2, providing a clear visual framework for subsequent analyses of different MPPT strategies.

2.1. Modeling of PV Cells

Accurate modeling of PV cells serves as a foundational requirement for both software simulations and data analysis, enabling the evaluation and verification of the operational performance of PV power generation systems [13]. Central to this modeling effort is the accurate prediction of the voltage-current (*V-I*) characteristic curve, which defines the electrical output profile of the PV cell. Notably, environmental variables, primarily solar irradiance and temperature, exert substantial influence on the cell's output voltage and current, as demonstrated by the comparative analyses in Figures 3 and 4. These fluctuations necessitate the use of adaptive modeling strategies to replicate real-world performance. To address this, researchers have developed diverse electrical circuit configurations that emulate PV module dynamics under shifting environmental parameters [14]. For instance, circuit models are designed to account for irradiance-dependent current generation and temperature-induced variations in semiconductor properties, enabling precise simulation of how modules respond to real-world operational stresses. By integrating these topological variations, models can better approximate the nonlinear relationships between environmental inputs and electrical outputs, ensuring reliable system evaluation across diverse climatic scenarios.

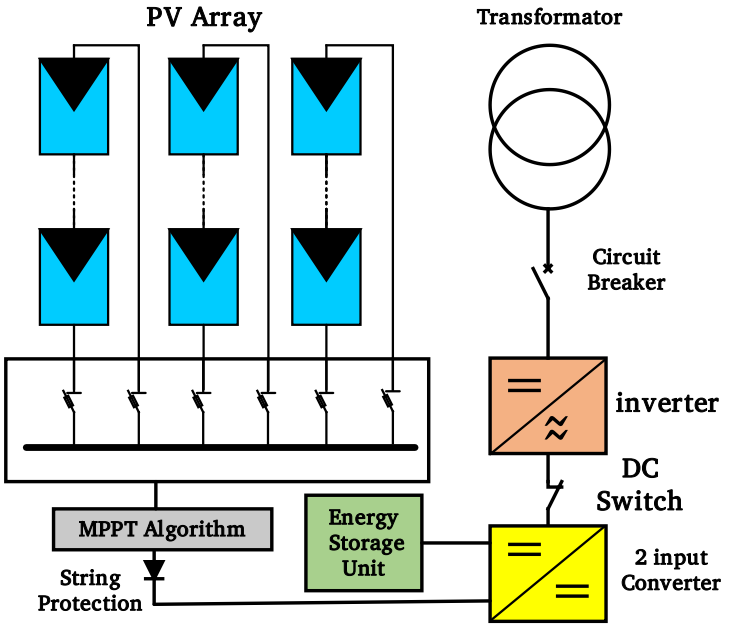

Figure 2. The configuration of the investigated PV system.

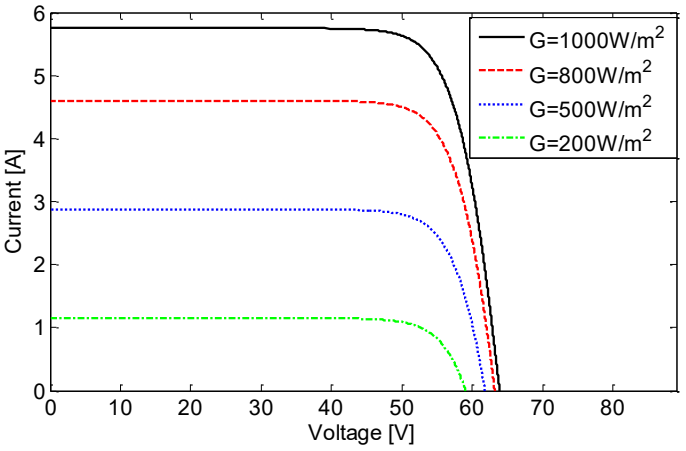

Figure 3. The influence of changes in ambient irradiation levels on the current-voltage (I–V) characteristics.

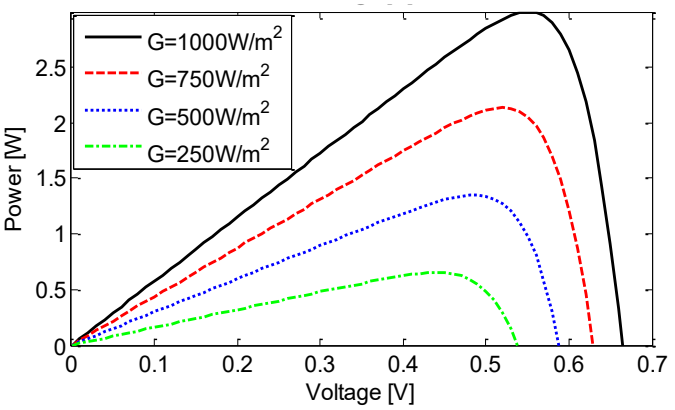

Figure 4. The effect of varying ambient irradiation levels on the characteristics of power-voltage (P–V) curve profiles.

Figure 5 illustrates the single-diode PV cell model, which utilizes an equivalent electrical circuit consisting of a light-sensitive current source, a diode, and two resistances, one in series and the other in shunt. This framework is mathematically defined by an adaptation of the Shockley diode equation [15], which accounts for resistive losses inherent to real-world PV cells. In this configuration: I_{ph} (photocurrent) quantifies the current generated by photon absorption in the semiconductor material. I_d (diode reverse saturation current) characterizes the leakage current under reverse bias, influenced by temperature and material properties. R_s (series resistance) represents resistive losses in metal contacts, busbars, and semiconductor bulk regions. R_{Sh} (shunt resistance) models leakage pathways across the cell's p-n junction, often caused by manufacturing defects. The interplay of these components governs the nonlinear voltage-current (*V-I*) relationship of the PV cell, formally expressed in Equation (1) [16]. This equation modifies the ideal diode law by incorporating voltage drops across R_s and current through R_{Sh}, enabling precise simulation of real-world cell behavior. For instance, R_s reduces the effective output voltage under high current loads, while R_{Sh} introduces parasitic losses at low irradiance levels. The accuracy of the model in reproducing empirical *V-I* curves (as shown in Figure 5) makes it indispensable for predicting performance degradation, optimizing MPPT algorithms, and evaluating efficiency losses under partial shading or aging effects.

$$I = N_P I_{Ph} - N_P I_d \left[exp\left(\frac{qV}{kTAN_S} - 1\right)\right] \quad (1)$$

Within PV system modeling, I (measured in amperes) defines the operational current produced by the PV array under load conditions, while V (in volts) represents the terminal voltage generated across the array's output. The architectural design of the PV system is shaped by two key parameters: 1) N_s: the count of solar cells connected in series, which scales the system's output voltage proportionally; and 2) N_p: the number of parallel-connected cell strings, which enhances current-carrying capacity to mitigate shading or mismatch losses. Fundamental physical constants embedded in the model include q (electron charge, $\sim 1.602 \times 10^{-19}$ C), governing charge carrier dynamics, and k (Boltzmann constant, $\sim 1.381 \times 10^{-23}$ J/K), linking thermal energy to semiconductor behavior. The dimensionless parameter A (ideality factor) quantifies deviations from ideal diode characteristics, reflecting recombination losses in the p-n junction. Values between 1 (ideal diode) and 5 (highly non-ideal) correlate with material defects, doping irregularities, or operating temperature extremes [17]. The reverse saturation current (I_d), representing leakage current under reverse bias, is temperature-dependent and influenced by minority carrier concentrations. It is derived analytically through Equation (2) [18], which incorporates material bandgap energy, intrinsic carrier density, and junction geometry.

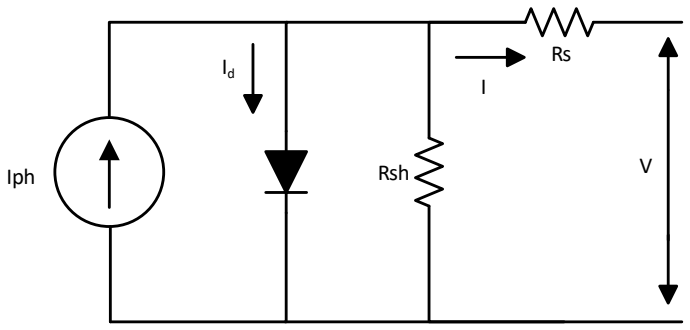

Figure 5. The single-diode equivalent circuit model for a PV cell.

Meanwhile, T (cell temperature in Kelvin) critically modulates both I_d and the thermal voltage (kT/q), with elevated temperatures reducing open-circuit voltage (V_{OC}) while marginally increasing short-circuit current (I_{SC}). This interdependence highlights the need for temperature-compensated MPPT algorithms in practical applications.

$$I_d = I_c[T/T_c]^3 exp\left[\left(q\frac{E_g}{KA}\right)\left(\frac{1}{T_c}-\frac{1}{T}\right)\right] \quad (2)$$

Within the PV cell's operational model, three critical parameters control temperature-dependent performance characteristics: T_C (reference temperature), I_c (reference saturation current) and E_g (band gap energy). These variables collectively determine the temperature-dependent behavior of the Shockley diode equation. For instance, E_g directly affects the temperature coefficient of I_c, as narrower bandgap materials exhibit stronger thermal degradation of V_{OC}. Meanwhile, deviations from T_C require recalibration of I_c to account for thermally accelerated carrier recombination, a process modeled in Equation (2). The interdependence of these parameters underscores their role in predicting efficiency losses under real-world thermal cycling conditions.

Equation (3) introduces a refined analytical framework for calculating the I_d in PV cells, explicitly addressing temperature-dependent carrier dynamics [19]. This enhanced formulation integrates three critical thermal effects: I) thermally activated carrier generation, which accounts for increased electron-hole pair generation at elevated temperatures, amplifying I_d through enhanced minority carrier concentrations; II) bandgap narrowing: models the temperature-induced reduction in semiconductor bandgap energy (E_g), which reduces the potential barrier for carrier recombination, directly influencing I_d exponential dependence on T, and III) non-ideal junction behavior: Incorporates temperature-dependent deviations from ideal diode characteristics via adjustments to the ideality factor (A), particularly under high-injection conditions. The equation resolves limitations in conventional I_d models by coupling these mechanisms through a multiplicative correction factor. For instance, it quantifies how a 10°C temperature rise in crystalline silicon cells increases I_d by approximately 7–9%, critically impacting MPP and maximum power (P_{max}) stability. By embedding these relationships, the model enables precise prediction of efficiency losses during thermal transients, such as midday irradiance spikes or partial shading-induced hot-spot heating. This advancement supports the design of temperature-resilient MPPT algorithms, particularly for grid-connected systems operating in climates with wide daily temperature variations.

$$I_d = \frac{q\left(I_{SC,T_c} + K_I\Delta T\right)}{exp\left[\left(V_{OC,T_c} + K_V\Delta T\right)/AKT\right] - 1} \quad (3)$$

Within this framework, the symbols I_{SC,T_c} and V_{OC,T_c} designate the short-circuit current and open-circuit voltage measured at a specific reference temperature, T_C. Here, K_I serves as the coefficient that characterizes how the short-circuit current adjusts with temperature changes, while K_V is the corresponding coefficient for the open-circuit voltage. The term ΔT, defined as $T - T_C$, quantifies the deviation between the current cell temperature, T, and the reference temperature, T_C. Additionally, the photocurrent (I_{ph}) mentioned in Equation (1) is sensitive to variations in both solar irradiation and the cell's temperature. Its variation with these factors is mathematically captured by the formula provided, which delineates the interplay between environmental conditions and the cell's electrical output. This formulation is critical for understanding and accurately modeling the behavior of photovoltaic cells under diverse operating conditions as in Equation (4).

$$I_{ph} = [I_{scr} + K_i(T - T_c)][S/100] \quad (4)$$

In this equation, I_{scr} represents the cell's short-circuit current measured at the reference temperature and a standard radiation level. K_i is the temperature coefficient that quantifies how the I_{scr} changes with variations of temperature, and S denotes the solar irradiation, expressed in mW/cm^2. Using these parameters, the total output power of the PV array can be calculated with the subsequent equation as in Equation (5).

$$P = V \times I \quad (5)$$

To determine the MPP of the array, the process begins by analyzing the variation in output power (P) in response to changes in voltage (V). The MPP is achieved when the rate of change of power with respect to voltage is zero, which we mathematically express as: $(dP/dV) = 0$. At this specific point, any infinitesimal change in voltage does not cause a corresponding change in power, indicating that the system is operating at its optimal condition. Deriving this zero-slope condition gives rise to the following equation that defines the MPP precisely in mathematical terms.

$$exp\left(\frac{qV_{max}}{KTAN_s}\right)\left[\left(\frac{qV_{max}}{KTAN_s}\right)+1\right]=\left(I_{ph}+I_d\right)/I_d \quad (6)$$

By rearranging Equation (5) algebraically, we derive V_{max}, representing the voltage at which the array achieves its peak power output. The output voltage generated by a PV cell is not an isolated phenomenon; it is inherently linked to the photocurrent produced within the cell. This photocurrent is primarily dictated by both the load current and the level of solar irradiation that the cell experiences during operation (refer to [15,20] for further details). The following equation presents this interdependent relationship, providing a clear mathematical framework for how these parameters work together to determine V_{max}.

$$V=\left(\frac{AKT}{a}\right)ln\left[\left(I_{ph}+I_d-I\right)/I_d\right]-R_sI \quad (7)$$

Adjusting solar radiation (S) and cell temperature (T) within Equations (1) to (6) enables the simulation of the $I-V$ and $P-V$ characteristics of a PV array [21]. A similar MATLAB-based simulation procedure for PV arrays, accounting for diverse shadow patterns and temperature conditions, was proposed in [22].

At the V_{OC}, the predictions of the single-diode model start to deviate significantly from experimental observations, particularly in scenarios with low irradiance levels [23]. This divergence highlights a significant limitation of the model, which is founded on the premise that recombination losses within the depletion region are negligible and can be disregarded. In reality, however, recombination plays a significant role as a source of loss in actual solar cells, its effect being particularly pronounced at lower voltage levels. Consequently, by disregarding these recombination losses, the single-diode model fails to accurately depict the cell's behavior when operating near V_{OC}, highlighting its inadequacy for precise modeling under such conditions [24].

2.2. PV Array Efficiency

The performance of a solar cell is determined by the complex interaction of key parameters such as solar irradiance, temperature, and overall resistance. This intricate relationship results in a non-linear dependency between the operating conditions and the efficiency of the cell. A primary method to analyze this behavior is through the current–voltage (I-V) characteristic curve, which captures how variations in these parameters affect the cell's performance. For instance, as demonstrated in Figures 3 and 4, an increase in solar irradiance leads to a significant boost in the short-circuit current, while the open-circuit voltage remains almost unchanged. In practical terms, because the peak power output is closely related to the short-circuit current, higher irradiation levels directly translate into increased power generation. Conversely, when the temperature elevates, the short-circuit current shows a modest increase; however, this is counterbalanced by a slight decline in the open-circuit voltage. Hence, the optimal power generation occurs at the precise intersection of the current source behavior and the voltage source behavior, a condition defined as the MPP. To ensure that the PV cells consistently operate at this optimal point, MPPT algorithms are employed. Despite these measures, PV systems encounter two primary challenges. The first challenge is that the conversion efficiency of generating electrical power remains relatively low, typically in the range of 9–25%, a situation that worsens under conditions of low irradiance. The second challenge is that the power output is inherently variable, as it continuously fluctuates with the changing patterns in the weather.

Analyzing MPPT behavior involves evaluating performance in both static and dynamic scenarios. In static conditions, MPPT efficiency specifically refers to the algorithm's ability to accurately detect and sustain the MPP when environmental factors, such as solar irradiance and temperature, are constant. Under these conditions, efficiency ($\eta_{inst}(t)$) is computed as an average over a predefined time interval once the system has reached a stable steady state. This stabilization period, or transient phase, may last several seconds, depending on the prevailing operating conditions. In contrast, dynamic MPPT efficiency considers the capability of the algorithm to continuously track the shifting MPP as environmental conditions vary. Here, the system's response is monitored in real time, and instantaneous efficiency is determined by comparing the actual measured power output against the ideal power output, theoretically calculated for the current level of irradiation. This calculation follows the formula provided in [25].

$$\eta_{inst}=\frac{P_{pv-meas}}{P_{MPP-ideal}}*100 \rightarrow for\ k\ \ number\ of\ samples: \frac{1}{k}\sum_{i=0}^{k}\frac{P_{pv-meas}}{P_{MPP-ideal}}*100 \quad (8)$$

In this framework, the symbol η_{inst} denotes the steady-state efficiency, which quantifies the PV system's performance under constant operating conditions. Meanwhile, $P_{pv-meas}$ refers to the actual power output produced by the solar panel, reflecting its real-world performance under the given circumstances. In contrast, $P_{MPP-ideal}$ represents the theoretical maximum power that the solar panel is capable of generating under ideal, controlled conditions. By recording the values of $P_{PV-meas-mean}$ and $P_{MPP-ideal-mean}$ during these dynamic tests, an equivalent efficiency can be exactly computed using the formula provided in [26].

$$\eta_{dynamic}=\frac{P_{pv-meas-mean}}{P_{MPP-ideal-mean}}*100 \quad 9)$$

In the given expression, the dynamic efficiency $\eta_{dynamic}$ is determined by comparing two averaged power values over the entire duration of the test. The first value is the mean of the measured power output $P_{PV-mean-mean}$ is obtained by recording the instantaneous power throughout the entire testing duration. The second value represents the average of the maximum power, $P_{MPP-ideal-mean}$, predicted by the PV model over the same period.

2.3. Comparative Evaluation of Set Point Tracking Across Various MPPT Techniques

A set point refers to a predefined target value that a control system aims to maintain or reach. When the controller employs set point tracking, it continuously adapts to align the target value with the current process value. In this paper, "set point tracking"

specifically refers to the process of continuously monitoring and maintaining the MPP as irradiation conditions change. For the offline evaluation, various techniques, namely OCV, SCC, and ANN, were simulated under dynamic irradiance conditions (see Figure 6 for the irradiance profiles). The corresponding outcomes of these simulations are displayed in Figure 7. The results clearly show that the ANN method is exceptionally precise in tracking the MPP when irradiance is variable. On the other hand, both the OCV and SCC approaches produce estimates of the MPP; however, the accuracy of them is compromised by interruptions in power supply. These disruptions can be attributed to the inherent need of the OCV and SCC approaches to measure the V_{OC} and I_{SC}, respectively. Among these, the SCC method offers better tracking performance compared to the OCV method. In addition to the offline techniques, the study also examined online methods, specifically, P&O and ESC, as well as hybrid strategies described in [11,12]. The simulation results presented in Figures 8 and 9 highlight notable variations in performance; while the P&O algorithm struggles to reliably follow the MPP during sudden shifts in irradiance, the ESC method, along with the hybrid techniques, demonstrates a considerably stronger ability to uphold the MPP under such dynamic conditions.

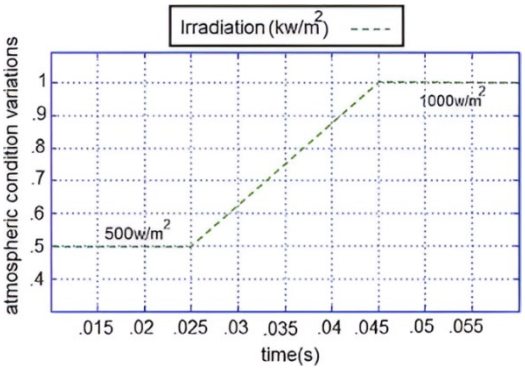

Figure 6. The dynamic patterns of solar irradiation over time.

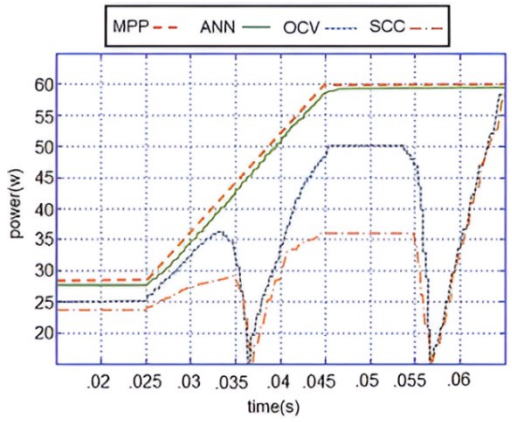

Figure 7. PV system output power under the offline MPPT method during dynamic irradiance conditions.

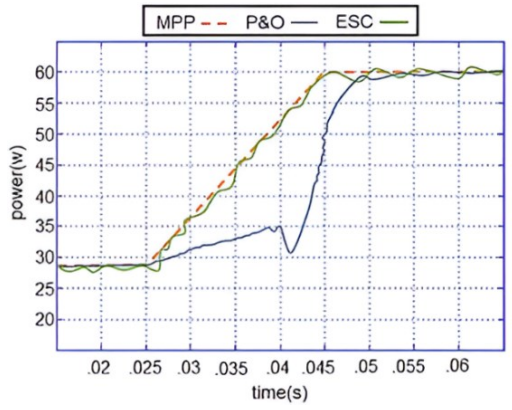

Figure 8. PV output power using online MPPT method under varying irradiance conditions.

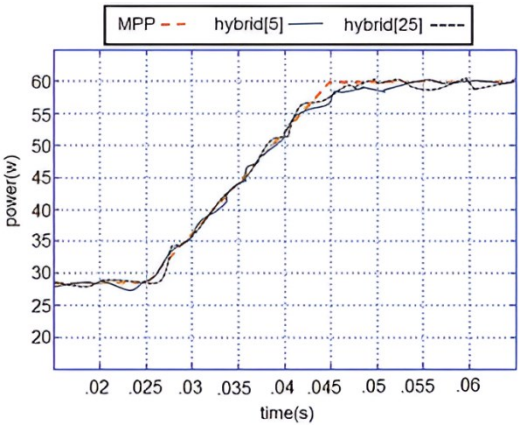

Figure 9. PV output power using a hybrid MPPT technique under fluctuating irradiance conditions.

Stability indices for the voltage output of PV systems are crucial in evaluating performance under varying conditions. Here are some notable indices used in assessing PV voltage stability: 1) Total voltage deviation index (TVDI): Measures fluctuations in the DC output voltage of PV systems. It helps assess system stability under dynamic conditions; voltage deviation refers to the variation between the output voltage of the PV system and the voltage at the MPP. A smaller deviation indicates improved voltage stability within the system. As expressed in Equation (10), the TVDI quantifies this deviation by summing the squared absolute differences between the PV output voltage and the MPP voltage across all PV arrays in the system. and 2) Dynamic voltage stability index (DVSI): Evaluates the ability of the PV system to maintain stable voltage under transient events such as sudden load changes or shading. A voltage recovery issue arises when the deviation in voltage exceeds 0.2, indicating instability in the system. The DVSI is computed based on Equation (11). In doing so, the voltage deviation for each PV panel is determined based on the steady-state voltage at the MPP condition. Based on the extracted shape of the TVDI, the graph corresponding to method hybrid [25] demonstrates excellent performance and maintains strong stability (see Figure 10). Additionally, methods hybrid [5], ESC, and ANN follow in terms of stability ranking. Furthermore, the results illustrated in Figure 11 for the (DVSI fully support this assessment.

$$TVDI = \sum_{i=1}^{N} |V_{PV-meas} - V_{MPP}|^2 \tag{10}$$

$$DVSI = \frac{V_{St}^{i} - V_{PV-meas}^{i}}{V_{c_t}^{i}} \tag{11}$$

Where N is the total number of PV panels, $V_{PV-meas}$ is the actual output voltage produced by the PV panels, V_{MPP} is the theoretical maximum voltage that the solar panel is capable of generating under MPP condition, and V_{St}^{i} is the actual steady-state voltage at the MPP condition.

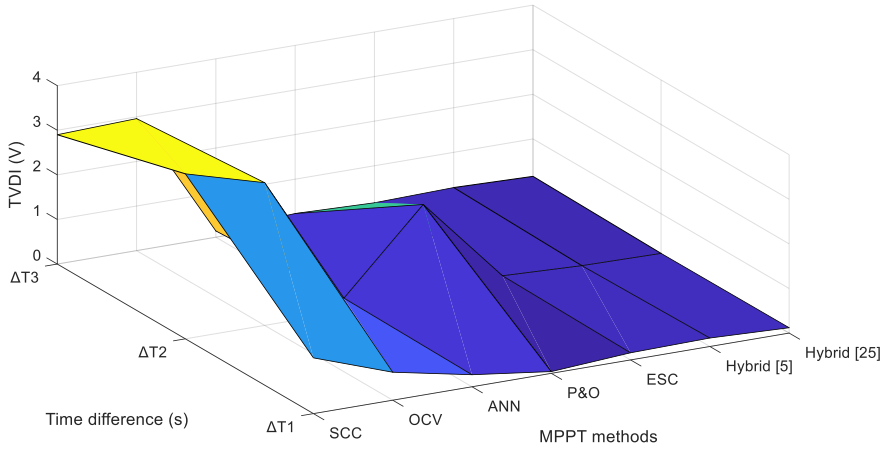

Figure 10. TVDI for a PV system utilizing various MPPT techniques under fluctuating irradiance conditions; $\Delta \boldsymbol{T_1} = \boldsymbol{0} < \boldsymbol{T} \leq \boldsymbol{0.025s}, \Delta \boldsymbol{T_2} = \boldsymbol{0.025s} < \boldsymbol{T} \leq \boldsymbol{0.045s}, \boldsymbol{T} > \boldsymbol{0.045s}$.

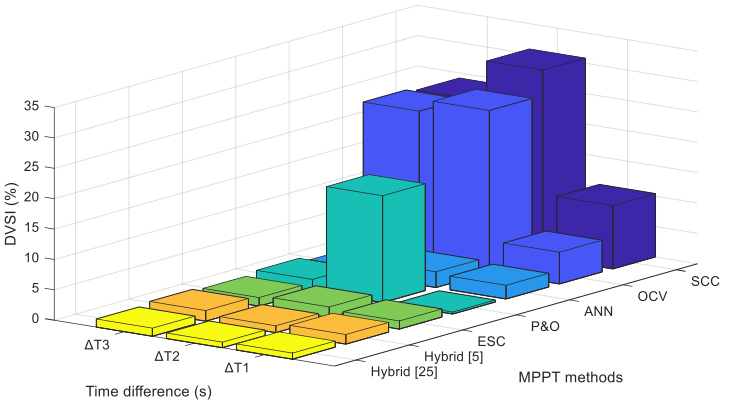

Figure 11. DVSI for a PV system utilizing various MPPT techniques under fluctuating irradiance conditions; $\Delta T_1 = 0 < T \leq 0.025s, \Delta T_2 = 0.025s < T \leq 0.045s, T > 0.045s$.

2.4. System Identification

We appreciate the respected referee's opinion and thank you for this question. System identification involves constructing empirical models of dynamic systems when their exact parameters or physical foundations are uncertain. This method generally implies that system dynamics can be estimated with high precision, eliminating the necessity for modeling. Hence, the primary objective of this method is to implement numerical optimization methods for model parameterization, enabling accurate prediction of nonlinear system behavior and stability analysis. Indeed, one of the key contributions of this article is the introduction of a comprehensive method that removes the necessity for dynamic modeling of the methods being analyzed. Without this innovation, it would be required to model the converter and then carry out dynamic modeling for each MPPT method under investigation. Consequently, system identification focuses on constructing mathematical models that reflect the inherent dynamics of a system by examining its input–output data. This process is crucial as it facilitates the creation of accurate models, which serve as a foundation for effective control strategies and reliable predictive analyses. So, to evaluate the dependability of the system, it is essential to identify its key parameters across a variety of atmospheric conditions. The RLS algorithm operates as an adaptive filter, adjusting its coefficients iteratively to reduce a weighted error based on the linear least squares principle associated with the input signals. In real-time applications, both the input and output data are processed sequentially at predetermined sampling intervals. Adaptive or self-adjusting control systems depend on continuously revising parameter estimates whenever new data samples are acquired. This continuous updating is typically achieved through online recursive strategies, which allow engineers to monitor and adjust parameter values as they evolve in real time. Owing to their computational efficiency, these recursive techniques are especially advantageous for implementation in microprocessor-based environments [27]. Furthermore, the dynamics of the transfer functions obtained in Equation (12) can be described by a linear difference equation that represents the relationship between the system's input and output.

$$G(Z^{-1}) = \frac{Y(Z^{-1})}{U(Z^{-1})} = \frac{b_1 + b_2 z^{-2} + b_3 z^{-3} + b_4 z^{-4} + \cdots + b_n z^{-n}}{1 + a_1 Z^{-1} + a_2 Z^{-2} + a_3 Z^{-3} + a_4 Z^{-4} + \cdots a_m Z^{-m}} \quad (12)$$

There are various approaches available to derive Equation (12); however, this work employs the relatively straightforward autoregressive exogenous (ARX) technique [28]. An ARX model integrates an autoregressive component with an exogenous input component to characterize and simulate the dynamic behavior of a system. By applying this method, the corresponding difference equation for the system's inputs and outputs can be formulated (see Equations (13) to (16)).

$$y(k) = -a_1 y(k-1) - a_2 y(k-2) - a_3 y(k-3) - \cdots - a_m y(k-m) + b_1 u(k-1) + b_2 u(k-2) + b_3 u(k-3) + \cdots + b_n u(k-n) + \lambda(k) \quad (13)$$

Within this framework, the notation y(k) represents the output signal, which corresponds to the power generated by the PV module. Conversely, u(k) denotes the input signal that captures the fluctuations in irradiance.

The sequence of parameters [a_1, a_2, …, a_n, b_1, b_2, …, b_n] comprises the coefficients that must be determined through estimation. In addition, the term $\lambda(k)$ is introduced as a white noise process with a normal distribution, characterized by a zero mean and a variance of 0.05, representing the random disturbances in the system.

$$\hat{\theta}(k) = \hat{\theta}(k+1) + \frac{P(k+1)\varphi(k)}{1 + \varphi^T(k)P(k-1)\varphi(k)} \times \varepsilon(k) \quad (14)$$

$$\varepsilon(k) = y(k) - \theta^T(k-1)\varphi(k) \quad (15)$$

$$P(k) = P(k-1) - \frac{P(k+1)\varphi(k)}{1 + \varphi^T(k)P(k-1)\varphi(k)} \times \varphi^T(k)P(k-1) \quad (16)$$

Within this framework, $y(k)$ is defined as the output power of the PV module. The regression vector $\varphi(k)$ encapsulates past and current input data, the estimated parameter vector $\hat{\theta}(k)$ contains the system's coefficients, and the prediction error $\varepsilon(k)$ quantifies

the difference between the model's output and the measured output. Moreover, $P(k)$ represents the covariance matrix associated with the estimation process.

To thoroughly analyze PV performance, output power data were collected over 730 hours from simulations using four distinct MPPT methods: ANN (typifying offline methods), P&O (representing online approaches), and two hybrid techniques as detailed in [11] and [12]. This comprehensive dataset was then utilized to build an ARX time series model, which has been determined to be the most effective for capturing the dynamic behavior of PV power. The parameters for each MPPT method, as derived from the ARX model, are presented as follows in Equations (17) to (20):

$$W_1(k) = 1.9874W_1(k-1) + 0.354W_1(k-2) - 0.5412W_1(k-3) + 0.4071u(k-1) + 0.987u(k-2) - 0.1004u(k-3) + \lambda(k) \quad (17)$$

$$W_2(k) = 1.305W_2(k-1) + 0.447W_2(k-2) - 0.369W_2(k-3) + 0.49811u(k-1) + 0.505u(k-2) - 0.0924u(k-3) + \lambda(k) \quad (18)$$

$$W_3(k) = 1.237W_3(k-1) - 0.0127W_3(k-2) + 0.347W_3(k-3) + 0.7151u(k-1) + 0.834u(k-2) - 0.121u(k-3) + \lambda(k) \quad (19)$$

$$W_4(k) = 0.924W_4(k-1) + 0.455W_4(k-2) - 0.612W_4(k-3) + 0.55051u(k-1) + 0.699u(k-2) - 0.1214u(k-3) + \lambda(k) \quad (20)$$

Here, $W_1(k)$, $W_2(k)$, $W_3(k)$, $W_4(k)$ represent the output power of the PV module, measured under each of the four MPPT strategies: the ANN method, the P&O method, and the two hybrid approaches as detailed in [11] and [12].

2.5. Reliability

This study utilizes the loss of load probability (LOLP) as a key metric to evaluate the reliability of the entire system. The LOLP serves as a measure to determine the probability that, during a defined timeframe (such as one month), the total energy demand will exceed the amount of power generated by the system. Leveraging this measure, the loss of load expectation (LOLE) can be derived. The LOLE estimates the average number of hours in a month during which an imbalance, caused by demand exceeding generation, is expected to occur. The calculation of LOLE is carried out using the formula provided in Equations (21) to (23).

$$LOLE = \sum_{i=1}^{730} [(W_t(i) + W_{batt}(i)) - P_l(i) < 0] \quad (21)$$

$$W_t(i) = W(k) - W_l \quad (22)$$

$$W(k) = -a_1W(k-1) - a_2W(k-2) - a_3W(k-3) - \cdots - a_mW(k-m) + b_1u(k-1) + b_2u(k-2) + b_3u(k-3) + \cdots + b_nu(k-n) + \lambda(k) \quad (23)$$

In this formula, the first parameter $W_t(i)$ denotes the validity coefficient of the PV module capacity, a factor that quantifies the effective capacity of the PV module under its operating conditions. Next, the term $W(k)$, representing actual power generation, refers to the real-time output of the entire PV module, fully accounting for the effects of irradiance variations throughout the statistical period for each MPPT method. Another parameter W_l in the formula corresponds to the power generation loss incurred due to PV module outages, capturing the impacts of any interruptions on energy yield. Additionally, W_{batt} defines the total power available from the battery pack when operating in discharge mode. Finally, $P_l(i)$ indicates the effective load power, which accounts for the gap between the demanded load and the losses in power generation that are influenced by the power grid.

3. Analysis of Simulation Outcomes and Interpretation

This section details the methodology employed to evaluate the performance of the PV system, focusing on its reliability and operational efficiency. The evaluation was carried out using four unique MPPT strategies, namely ANN, P&O, and two hybrid techniques as described in the studies cited in [11,12]. All the simulations were executed within the MATLAB software environment. A critical aspect of assessing the impact of the different MPPT strategies on the PV system's reliability is the precise modeling of solar irradiation. Since irradiation exhibits continuous fluctuations and varies with geographic location, capturing these dynamics accurately is essential.

To achieve this, an irradiance model is implemented, precisely simulating the temporal variations of solar energy over a predetermined period. For the specific PV system under analysis, the model generated simulations of daily solar irradiation patterns, as depicted in Figure 12. Based on these data, Figure 13 provides a detailed comparison of the evaluated efficiency as a function of PV output power for the various MPPT techniques under study. The performance of a PV system in generating electricity is heavily influenced by weather conditions. While maximum power is generated on sunny days, sudden cloud-induced shading diminishes both efficiency and output.

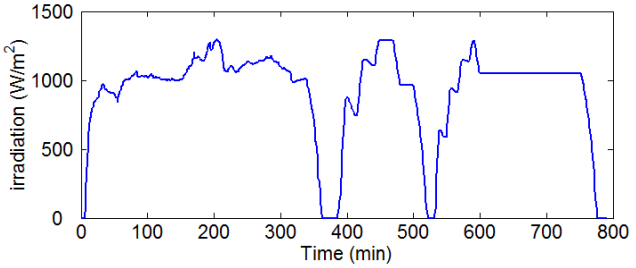

Figure 12. Variation of solar irradiation.

Shading refers to any obstruction that prevents sunlight from reaching the PV panels and can also result from accumulated dust, which gradually reduces system efficiency. Additionally, the efficiency and output of a PV system are influenced by various factors, such as increased temperatures and abrupt changes in irradiance. Therefore, an effective MPPT algorithm is essential to enhance system performance, ensuring maximum power tracking and addressing these issues.

In this illustration, each curve shown in Figure 13 represents the efficiency performance of its respective MPPT method as the output power from the PV module changes. It is important to note that this efficiency diagram is derived under idealized conditions, excluding any losses attributed to secondary power stage components. Specifically, the diagram omits reductions due to power semiconductor device losses, the inherent losses in the output inductor, and the power consumption attributed to both the control circuit and its associated driver circuit. This exclusion allows for a focused evaluation of the intrinsic performance of the MPPT strategies, isolating the impact of the MPPT algorithm on the PV system's efficiency without interference from losses in the main power conversion components. Tables 1 to 4 present the operating performance and key metrics of a PV power generation system when the different MPPT approach is applied.

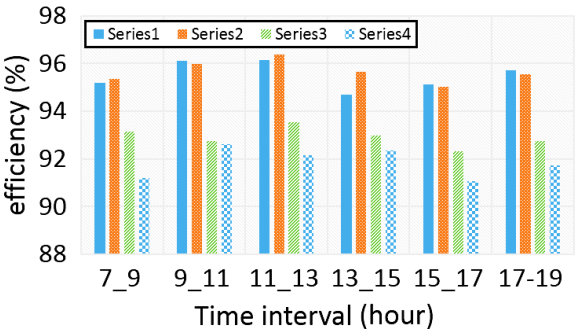

Figure 13. The measured conversion efficiency of the PV system as a function of its output power. Series 1 represents the hybrid method [11], series 2 represents the hybrid method [12], series 3 corresponds to the P&O method, and series 4 corresponds to the ANN method.

Table 1. Operating performance and key metrics of a PV module when applying the ANN MPPT approach.

Solar irradiance (W/m^2)	The PV power capacity (W)	
	in	out
900-1000	10100	900
800-900	9780	1200
700-800	9150	1850
600-700	8340	2660
500-600	7260	3740
400-500	7015	3985
300-400	6740	4260
200-300	6420	4580
100-200	6229	4771

Table 2. Operating performance and key metrics of a PV module when applying the P&O MPPT approach.

Solar irradiance (W/m2)	The PV power capacity (W)	
	in	out
900-1000	10350	650
800-900	10020	980
700-800	9089	1911
600-700	8979	2021
500-600	8445	2555
400-500	7565	3435
300-400	6730	4270
200-300	6659	4341
100-200	6467	4533

Table 3. Operating performance and key metrics of a PV module when applying the hybrid [11] MPPT approach.

Solar irradiance (W/m2)	The PV power capacity (W)	
	in	out
900-1000	10778	212
800-900	10410	590
700-800	9961	1039
600-700	9473	1527
500-600	9156	1844
400-500	8567	2433
300-400	8008	2992
200-300	7352	3648
100-200	7011	3989

The comparative analysis illustrated in Figure 14 reveals that incorporating hybrid MPPT strategies into the PV system consistently improves the LOLE metric. This finding highlights that hybrid approaches effectively reduce load loss, thereby enhancing the system's overall reliability. A detailed examination of these indices indicates that applying hybrid MPPT methods, rather than solely relying on offline or online techniques, leads to significant changes in the average duration of annual outages. However, the analysis also reveals that as hybrid methods are increasingly adopted, the degree of improvement in the load point's LOLE under PV power conditions gradually diminishes.

4. Distribution System Studies

The primary objective of electrical power systems is to supply electricity to consumers in a manner that is both reliable and cost-effective. Simply put, the reliability of the system reflects its ability to consistently meet energy demands by delivering the required electricity. To evaluate performance, a set of metrics known as electric power distribution reliability indices [29] is utilized to assess the behavior of electrical distribution networks. Central to reliability assessments of electrical distribution systems are parameters that quantify their operational performance over time. These parameters include the average failure rate (denoted as λ), which represents the frequency at which system components fail within a specified time frame. It provides critical insight into the overall reliability of the network's infrastructure. Another significant parameter is the typical outage duration (denoted as r), which reflects the average amount of time required to restore functionality after a failure occurs. This metric is pivotal for evaluating the efficiency of maintenance and repair processes. Additionally, the average annual outage time (denoted as U) measures the cumulative time over a year during which the system is unavailable or not meeting energy demands. This value is essential for assessing the long-term performance and impact of outages on consumers and operations.

These variables are typically derived by employing statistical models, such as exponential distribution models, which are widely used in reliability engineering. These models estimate the likelihood of failure and repair times by analyzing the time intervals between successive failures and the durations needed for repairs. The exponential distribution assumes that events occur at a constant rate, making it well-suited for scenarios where failure and repair events are random but follow predictable patterns. This methodology is detailed mathematically in Equations (24) to (26), where the relationships between failure rates, outage durations, and cumulative outage times are formulated to ensure accurate and comprehensive evaluations of system reliability.

Among the critical indices utilized in utility systems to assess reliability are the system average interruption frequency Index (SAIFI) and the system average interruption duration index (SAIDI). SAIFI provides a measure of the frequency of service interruptions by calculating the average number of outages experienced by individual customers within a given time frame. This index is essential for determining the regularity of disruptions and identifying areas where infrastructure improvements may be needed. In contrast, SAIDI evaluates the cumulative duration of these interruptions, representing the average time customers are without electricity during outages. This metric is pivotal for understanding the impact of service disruptions in solar systems on customer satisfaction and operational efficiency. Table 5 offers a comprehensive summary of the primary indices applied in assessing the performance of electrical power systems considering solar power generation.

Table 4. Operating performance and key metrics of a PV module when applying the hybrid [12] MPPT approach.

Solar irradiance (W/m2)	The PV power capacity (W)	
	in	out
900-1000	10533	467
800-900	10256	744
700-800	10002	998
600-700	9467	1533
500-600	9139	1861
400-500	8733	2267
300-400	8144	2856
200-300	7466	3534
100-200	7109	3891

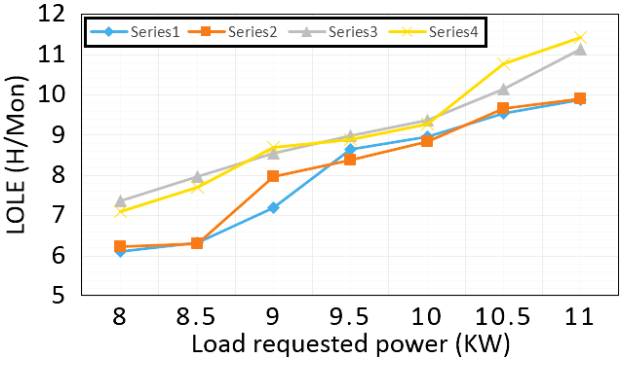

Figure 14. The LOLE, expressed in hours per month, for a PV module under different load requirements. The graph is divided into four series corresponding to the different MPPT methods. Series 1 to 4 represent the same methods as described in Figure 11.

These indices serve as valuable tools for utility providers to monitor, evaluate, and enhance the reliability and efficiency of their networks, ensuring consistent and dependable power delivery to consumers.

$$\lambda_s = \sum_{i=1} \lambda_j \tag{24}$$

$$U_s = \sum_{i=1} \lambda_j r_j \tag{25}$$

$$r_s = \frac{U_s}{\lambda_s} = \frac{\sum_{j=1} \lambda_j r_j}{\sum_{i=1} \lambda_i} \tag{26}$$

As shown in Figure 15, the distribution system used to analyze the impact of MPPT methods on reliability indices consists of 4 main feeders, 31 primary lines, 73 lateral lines, and 54 load points. A total of 3,080 customers are connected across all feeders. Each feeder includes a variety of components, such as lines, breakers, disconnect switches, and fuses. The primary system components are distribution lines or a combination of lines with disconnect switches, while lateral system parts typically include lines, fuses, or their combinations. Additional system specifications are detailed in Table 6.

The process of repair and switching within the system is characterized using log-normal distributions to reflect the inherent variability in response times. Specifically, the repair duration for power lines follows a log-normal distribution with a standard deviation of 4 hours, capturing the fluctuations in maintenance efforts due to varying conditions such as weather, accessibility, and resource availability. Likewise, the switching times associated with system elements are modeled using the same statistical distribution, but with a much lower standard deviation of 0.4 hours, highlighting the relatively swift nature of reconfiguration actions.

In terms of failure rates, the probability of faults occurring in lines and cables is largely dependent on their physical lengths (L), as longer segments are exposed to greater environmental stresses and potential points of failure. The primary feeder sections, those responsible for transmitting electricity along the main network pathways, are subject to failure rates quantified by the formula ($L \times 0.075$) faults per kilometer per year ($f/km-yr$). In contrast, lateral distribution lines, which typically branch off to supply individual sectors or consumers, experience a slightly higher failure rate of ($L \times 0.097$) faults per kilometer per year, likely due to their exposure to more complex operational conditions and external disturbances.

To provide a comprehensive overview of system reliability and performance, the fundamental indices for each load point are systematically documented in Table 7. This table presents key reliability metrics, such as outage frequencies and durations, enabling a detailed assessment of service continuity across different segments of the network. Additionally, Table 8 outlines the respective line lengths, which serve as crucial parameters for evaluating the maintenance requirements within the system.

Table 5. Distribution system reliability indices [29]

System Average Interruption Frequency (SAIFI)	$SAIFI = \frac{\sum \lambda_j N_j}{\sum N_i}$
System Average Interruption Duration Index (SAIDI)	$SAIDI = \frac{\sum U_j N_j}{\sum N_i}$
Customer Average Interruption Duration Index (CAIDI)	$CAIDI = \frac{\sum U_j N_j}{\sum \lambda_i N_i}$
Average Service Availability Index (ASAI)	$ASAI = \frac{\sum N_j \times 8760 - \sum U_j N_j}{\sum N_i \times 8760}$
Average Energy Not Supplied (AENS)	$AENS = \frac{\sum L_a(j) U_j}{N_i}$
* 8760 is the number of hours in a calendar year	

Table 6. Specification for the test distribution system of Figure 13.

Load Points	Load Level per Load Point (MW)		Number of Customers
	Peak	Average	
1, 3, 5, 7, 37, 41	0.74114	0.56369	15
8, 35, 36, 48, 52	0.48712	0.39647	130
9-12, 38-40	0.74651	0.61279	25
2, 4, 6, 44, 46, 49, 53	1.10459	0.96781	10
13, 15, 29-31	0.84562	0.63647	55
17-20, 27, 28	0.60073	0.41136	30
14, 16, 42, 50, 51	1.23349	1.00127	25
21, 22, 32-34, 54	0.47126	0.37719	45
24, 26, 43	0.54557	0.41879	210
23, 25, 45, 47	0.73267	0.55264	160

Table 7. Line types and lengths.

Line numbers	Type	Length (km)
1, 3, 5, 7, 9, 11	main	0.85
13, 24, 26, 28, 30, 40, 42	main	0.9
45, 51, 53, 55, 67, 69	main	0.7
72, 74, 76, 78, 80, 82	main	0.95
93, 95, 97, 99, 101, 103	main	0.75
0, 2, 4, 6, 8, 10, 12, 83, 85	lateral	0.35
15, 17, 19, 21, 23, 94, 98, 102	lateral	0.5
14, 31, 33, 46, 56, 62	lateral	0.45
25, 27, 29, 41, 43, 44, 52, 54, 68, 70, 92, 96, 100, 104	lateral	0.6
32, 34-39, 47, 49, 57, 59, 61, 63, 65, 84, 86-91	lateral	0.4
16, 18, 20, 22, 48, 50, 58, 60, 64, 66	lateral	0.65
71, 73, 75, 77, 79, 81	lateral	0.5

To assess the impact of MPPT techniques on the reliability of grid-connected PV systems, consider a scenario in which the PV unit serves as a load transfer mechanism. This means that the PV system dynamically adjusts its power output based on the MPPT algorithm it employs, thereby influencing how effectively it compensates for load fluctuations and contributes to overall grid stability.

In this context, the outage duration following a failure event is directly influenced by the ability of the PV unit to sustain or exceed the required load demand. Specifically, if the MPPT algorithm enables the PV unit to generate adequate power to meet the load requirement during the failure period, the outage time is limited to the isolation time, the duration needed to disconnect the affected component from the network and stabilize operations. This scenario assumes that the PV system continues to supply uninterrupted power to the load, preventing an extended outage.

Conversely, if the PV unit fails to deliver sufficient power due to either inefficiencies in MPPT tracking or unfavorable operating conditions (such as shading, temperature fluctuations, or transient changes in irradiance), the outage time is determined by the required repair duration. In this case, the affected component remains out of service until restoration efforts are completed.

To quantify the reliability impact of different MPPT techniques, the average outage time can be estimated using the expectation concept as Equation (27), integrating the probabilities of each scenario. Mathematically, this expectation-based approach captures the likelihood-weighted contributions of both isolation and repair times, allowing for a comparative evaluation of various MPPT algorithms in terms of system resilience and service continuity.

$$Outage\ time = (outage\ time \mid PV\ unit\ can\ generate\ enough\ power) \times P(generate) + (outage\ time \mid PV\ unit\ cannot\ generate\ enough\ power) \times Q(generate) \quad (27)$$

It is important to note that $P(generate)$ is significantly influenced by the performance of the PV unit (output power based on the applied MPPT methods) and the extent of the outage, particularly the number of customers impacted by the feeder outages.The comprehensive evaluation of reliability indices for the distribution PV-grid, as depicted in Figure 13, presents a comparative analysis across various MPPT algorithms. These indices, derived through analytical methodologies, provide critical insights into how different MPPT strategies influence the operational stability and dependability of the grid-integrated PV system.

One of the key observations from Table 9 is that all examined scenarios maintain an identical SAIFI. This consistency indicates that regardless of the MPPT algorithm employed, the frequency of interruptions remains uniform across the system. However, while the occurrence of interruptions remains unchanged, significant variations are observed in reliability indices related to interruption duration, highlighting the role MPPT strategies play in determining the length of outages.

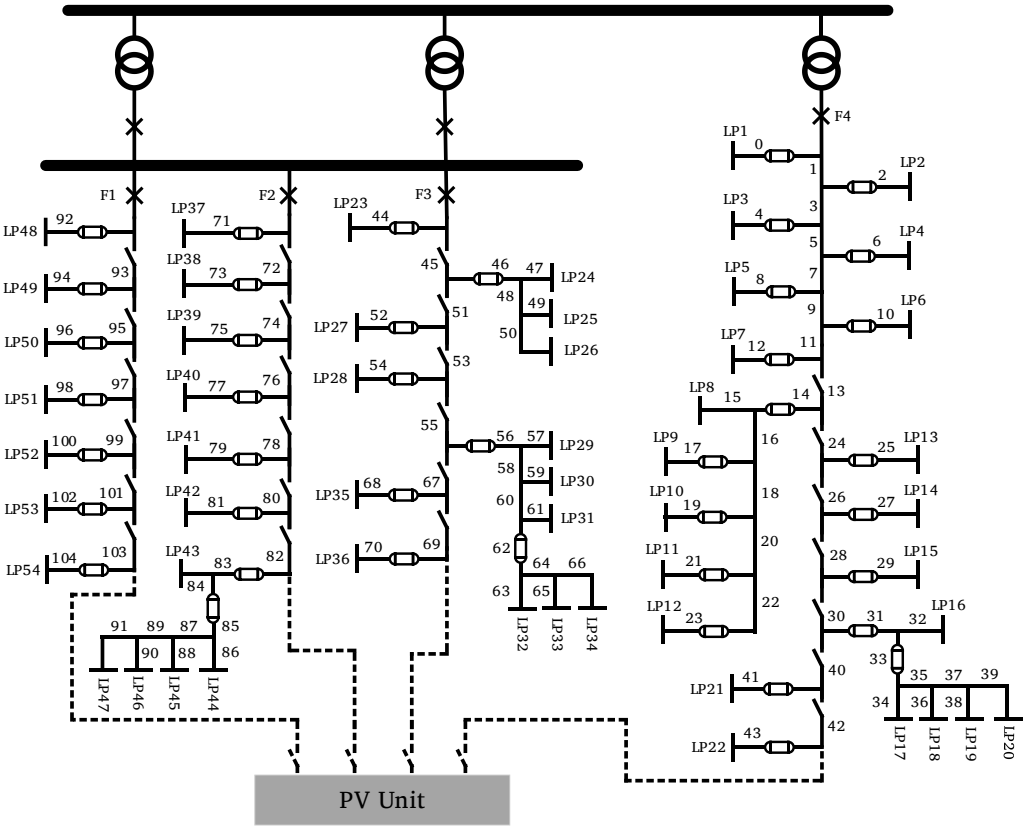

Figure 15. Test distribution system.

Table 8. The basic system indices for the distribution systems for each load point in different modes of MPPT algorithms for PV units (for load points 37-47, the calculation is set as given in the Appendix)

MPPT Method	ANN			P&O			Hybrid method [11]			Hybrid method [12]		
Load Point	λ	r	U	λ	r	U	λ	r	U	λ	r	U
1	1.2375	3.3342	4.1261	1.2375	3.2657	4.0413	1.2375	3.1014	3.8379	1.2375	3.1665	3.9185
2	1.2375	3.3342	4.1261	1.2375	3.2657	4.0413	1.2375	3.1014	3.8379	1.2375	3.1665	3.9185
3	1.2375	3.3342	4.1261	1.2375	3.2657	4.0413	1.2375	3.1014	3.8379	1.2375	3.1665	3.9185
4	1.2375	3.3342	4.1261	1.2375	3.2657	4.0413	1.2375	3.1014	3.8379	1.2375	3.1665	3.9185
5	1.2375	3.3342	4.1261	1.2375	3.2657	4.0413	1.2375	3.1014	3.8379	1.2375	3.1665	3.9185
6	1.2375	3.3342	4.1261	1.2375	3.2657	4.0413	1.2375	3.1014	3.8379	1.2375	3.1665	3.9185
7	1.2375	3.3342	4.1261	1.2375	3.2657	4.0413	1.2375	3.1014	3.8379	1.2375	3.1665	3.9185
8	1.3079	2.9567	3.8671	1.3079	2.8114	3.6770	1.3079	2.7994	3.6613	1.3079	2.8002	3.6623
9	1.3214	2.9634	3.9158	1.3214	2.8746	3.7984	1.3214	2.8201	3.7264	1.3214	2.8255	3.7336
10	1.3214	3.1219	4.1252	1.3214	3.0989	4.0948	1.3214	3.0149	3.9839	1.3214	3.0154	3.9845
11	1.3214	3.1978	4.2256	1.3214	3.0012	3.9657	1.3214	2.9872	3.9472	1.3214	2.9901	3.9511
12	1.3214	3.2416	4.2834	1.3214	3.1137	4.1144	1.3214	3.0134	3.9819	1.3214	3.0123	3.9804
13	1.3299	2.1827	2.9027	1.3299	2.0999	2.7926	1.3299	2.0057	2.6673	1.3299	2.0061	2.6679
14	1.3299	2.2789	3.0307	1.3299	2.1213	2.8211	1.3299	2.0639	2.7447	1.3299	2.0657	2.7471
15	1.3299	2.2999	3.0586	1.3299	2.1997	2.9253	1.3299	2.1482	2.8569	1.3299	2.1493	2.8583
16	1.3357	3.1149	4.1605	1.3357	3.0112	4.0220	1.3357	2.9901	3.9938	1.3357	2.9976	4.0039
17	1.3368	3.1477	4.2078	1.3368	3.1009	4.1452	1.3368	2.9842	3.9892	1.3368	2.9912	3.9986
18	1.3368	3.2007	4.2786	1.3368	3.1145	4.1634	1.3368	3.0997	4.1437	1.3368	3.1006	4.1449
19	1.3368	3.2034	4.2823	1.3368	3.1553	4.2180	1.3368	3.1005	4.1447	1.3368	3.1094	4.1566
20	1.3368	3.2101	4.2912	1.3368	3.1412	4.1991	1.3368	3.1497	4.2105	1.3368	3.1572	4.2205
21	1.3401	3.4141	4.5752	1.3401	3.2998	4.4220	1.3401	3.2012	4.2899	1.3401	3.2106	4.3025
22	1.3401	3.4141	4.5752	1.3401	3.2998	4.4220	1.3401	3.2012	4.2899	1.3401	3.2106	4.3025
23	0.7354	1.9746	1.4521	0.7354	1.8544	1.3637	0.7354	1.7433	1.2820	0.7354	1.7591	1.2936
24	0.7397	2.1211	1.5690	0.7397	2.1002	1.5535	0.7397	1.9819	1.4660	0.7397	1.9893	1.4714
25	0.7401	2.2723	1.6817	0.7401	2.2521	1.6667	0.7401	2.1464	1.5885	0.7401	2.1401	1.5839
26	0.7397	2.3009	1.7019	0.7397	2.2808	1.6871	0.7397	2.2017	1.6286	0.7397	2.2135	1.6373
27	0.7412	2.0017	1.4836	0.7412	1.9869	1.4727	0.7412	1.9832	1.4699	0.7412	1.9907	1.4755
28	0.7445	2.0179	1.5023	0.7445	1.9912	1.4824	0.7445	1.9517	1.4530	0.7445	1.9635	1.4767
29	0.7509	2.4712	1.8556	0.7509	2.3712	1.7805	0.7509	2.3113	1.7356	0.7509	2.3214	1.7431
30	0.7512	2.3625	1.7747	0.7512	2.3417	1.7591	0.7512	2.3146	1.7387	0.7512	2.3264	1.7476
31	0.7509	2.2525	1.6914	0.7509	2.2405	1.6824	0.7509	2.2135	1.6621	0.7509	2.2247	1.6705
32	0.7526	2.6839	2.0199	0.7526	2.6151	1.9681	0.7526	2.5146	1.8925	0.7526	2.5207	1.8970
33	0.7533	2.7494	2.0711	0.7533	2.7295	2.0561	0.7533	2.6319	1.9826	0.7533	2.6392	1.9881
34	0.7526	2.7506	2.0701	0.7526	2.7351	2.0584	0.7526	2.7019	2.0334	0.7526	2.7084	2.0376
35	0.7412	2.1468	1.5912	0.7412	2.1255	1.5754	0.7412	2.0197	1.4970	0.7412	2.0236	1.4998
36	0.7412	2.1468	1.5912	0.7412	2.1255	1.5724	0.7412	2.0197	1.4970	0.7412	2.0236	1.4998
37	0.47600	0.7668	0.36499	0.4760	0.7573	0.3604	0.4760	0.7211	0.3432	0.4760	0.7305	0.3477
38	0.47600	1.3057	0.62150	0.4760	1.2996	0.6186	0.4760	1.2514	0.5956	0.4760	1.2584	0.5989
39	0.47600	1.4868	0.70771	0.4760	1.47117	0.7003	0.4760	1.4312	0.6812	0.4760	1.4398	0.6853
40	0.47600	1.6679	0.79392	0.4760	1.65979	0.7901	0.4760	1.6113	0.7669	0.4760	1.6183	0.7703
41	0.47600	1.8490	0.88012	0.4760	1.8490	0.8801	0.4760	1.8112	0.8621	0.4760	1.8187	0.8657
42	0.47600	2.0301	0.96635	0.4760	2.0219	0.9624	0.4760	1.9963	0.9502	0.4760	1.9989	0.9514
43	0.50025	2.2979	1.14956	0.50025	2.2817	1.1414	0.50025	2.2317	1.1164	0.50025	2.2384	1.1197
44	0.76700	2.8899	2.21656	0.7670	2.8703	2.2015	0.7670	2.8243	2.1662	0.7670	2.8305	2.1710
45	0.76700	2.8899	2.21656	0.7670	2.8703	2.2015	0.7670	2.8243	2.1662	0.7670	2.8305	2.1710
46	0.76700	2.8899	2.21656	0.7670	2.8703	2.2015	0.7670	2.8243	2.1662	0.7670	2.8305	2.1710
47	0.76700	2.8899	2.21656	0.7670	2.8703	2.2015	0.7670	2.8243	2.1662	0.7670	2.8305	2.1710
48	0.39571	1.44127	0.57032	0.39571	1.4319	0.5666	0.39571	1.4011	0.5544	0.39571	1.4094	0.5577
49	0.38600	1.01261	0.39086	0.38600	1.00556	0.3881	0.38600	0.9964	0.3846	0.38600	1.0003	0.3861
50	0.39571	1.59762	0.63219	0.39571	1.59001	0.6291	0.39571	1.5517	0.6140	0.39571	1.5582	0.6166
51	0.38600	1.69753	0.65524	0.38600	1.68775	0.6514	0.38600	1.6429	0.6341	0.38600	1.6504	0.6370
52	0.39375	1.89998	0.74812	0.39375	1.89067	0.7444	0.39375	1.8732	0.7376	0.39375	1.8806	0.7404
53	0.38600	2.01813	0.77900	0.38600	2.00311	0.7732	0.38600	1.9864	0.7667	0.38600	1.9913	0.7686
54	0.39570	2.22307	0.87967	0.39570	2.21547	0.8766	0.39570	2.1468	0.8495	0.39570	2.1355	0.8450

These differences are further illustrated in Figure 16, which visually demonstrates how each MPPT algorithm affects the system's reliability metrics. The results suggest that selecting the most efficient MPPT technique can substantially influence unavailability indices, a crucial factor in assessing the continuous availability of power supply at load points. Furthermore, an optimal MPPT approach has a direct impact on the expected energy not supplied (EENS), which quantifies the amount of energy that remains unavailable due to system disruptions. This metric is especially relevant for grid planners and operators seeking to minimize the adverse effects of power shortages.

Given these findings, the development and refinement of an optimized MPPT methodology becomes imperative, not only for enhancing system reliability but also for facilitating a thorough cost-benefit analysis of PV unit deployment. A well-calibrated MPPT technique can lead to improved energy extraction efficiency, reduced outage durations, and an overall increase in power system resilience. Thus, further research into adaptive MPPT strategies and predictive control mechanisms may prove instrumental in maximizing the performance of grid-connected PV systems while ensuring their economic viability.

The cost of a PV system is closely linked to the number of sensors required for monitoring and control. Sensors play a crucial role in ensuring the accurate tracking of electrical parameters, but their quantity and type directly influence the overall expense of the system. In general, voltage measurement is considered simpler, more reliable, and less costly compared to current measurement. This distinction arises due to the inherent complexities in current sensing technologies, which often involve precision components such as Hall-effect sensors or shunt resistors. These components can be relatively expensive and may introduce additional calibration and maintenance requirements.

This cost consideration becomes particularly significant in multi-array PV systems, where each PV array is equipped with its own MPP tracker [30]. In such configurations, the need to monitor individual current outputs from multiple arrays can dramatically increase the total number of required sensors, further inflating system costs. The complexity of implementing multiple current sensors, along with the associated data acquisition and processing requirements, can pose logistical and financial challenges. To mitigate these concerns, an alternative approach involves adopting MPPT methods that either minimize sensor dependency or rely on voltage-based estimations to infer current behavior. Certain advanced MPPT strategies, as demonstrated in [31], leverage mathematical models and algorithmic approximations to estimate current from voltage measurements, reducing the necessity for direct current sensing. These techniques optimize system performance while maintaining cost efficiency, making them particularly advantageous for large-scale PV deployments.

By implementing sensor-efficient MPPT methodologies, system designers can achieve a balance between performance, reliability, and cost-effectiveness, ensuring that photovoltaic arrays operate efficiently without unnecessary expenses linked to excessive sensor integration. Continued research in this domain may lead to further refinements in MPPT algorithms, enabling even more precise estimations of electrical parameters with minimal hardware requirements.

High-cost applications like solar vehicles, industrial systems, and large-scale residential setups typically prioritize accuracy and fast response times, necessitating advanced and complex circuit designs. On the other hand, simpler and more affordable MPPT techniques are suitable for applications such as small residential systems or water pumping for irrigation. Given these considerations, it is challenging to determine the exact monetary cost of each MPPT technique without actual implementation. However, in general, analog implementations are more cost-effective than digital ones, which often require a microcontroller and related programming.

Addressing cost challenges in PV distribution systems requires the integration of advanced reliability cost/worth evaluation techniques into both system design and operational frameworks. These evaluation methods aim to balance economic feasibility with system performance, ensuring that PV installations maintain high efficiency while minimizing unnecessary expenditures. By incorporating cost-benefit analysis approaches, decision-makers can effectively determine the most suitable MPPT strategies based on reliability, implementation complexity, and return on investment. Based on overall implementation considerations, MPPT methods can be ranked as follows: 1) P&O; 2) hybrid methods; and 3) ANN.

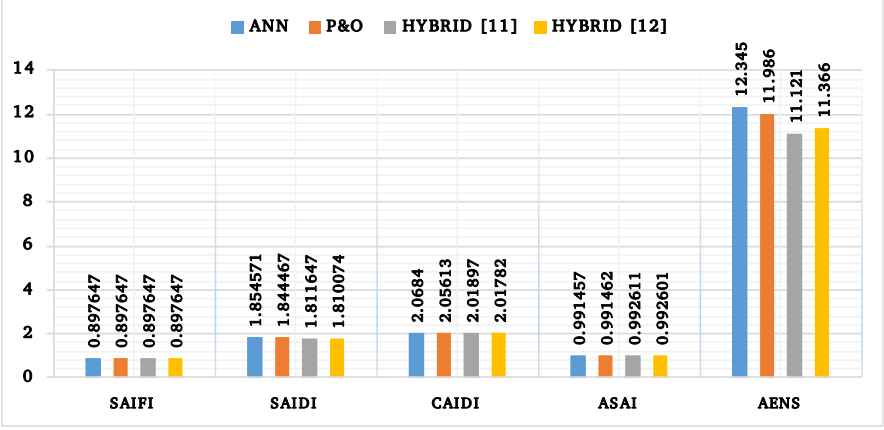

Figure 16. The differences in the reliability indices for each MPPT algorithm.

Table 9. The differences in the reliability indices.

Reliability Indices	MPPT Method			
	ANN	P&O	Hybrid method [11]	Hybrid method [12]
(SAIFI)	0.897647	0.897647	0.897647	0.897647
(SAIDI)	1.854571	1.844467	1.811647	1.810074
(CAIDI)	2.0684	2.05613	2.01897	2.01782
(ASAI)	0.991457	0.991462	0.992611	0.992601
(AENS)	12.345	11.986	11.121	11.366

5. Conclusion and Future Works

This study investigated the impact of various MPPT methods on the operational reliability of PV systems operating in grid-connected mode. The analysis classified MPPT methods into three distinct categories: offline, online, and hybrid methods, enabling a comprehensive assessment of their performance characteristics. To comprehensively assess system performance, a series of simulations was conducted to evaluate three critical metrics: reliability, efficiency, and set-point tracking. These factors play a pivotal role in determining the operational robustness and effectiveness of the implemented methodologies. Specifically, various offline, online, and hybrid methods were compared under similar implementation conditions. This rigorous analysis provided valuable insights into the practical performance of each strategy. The results demonstrated that hybrid methods significantly outperformed both standalone offline and online techniques. A key factor behind their superior performance is the reliance of online methods on real-time output sampling, which tracks the MPP by monitoring electrical parameters without requiring predefined system parameters, allowing for rapid adaptation to changes. By integrating these fast-response online techniques within a hybrid framework, the stability and robustness of offline strategies are combined, resulting in enhanced overall performance. These findings indicate that further optimization and adoption of hybrid MPPT strategies could substantially improve the performance and reliability of grid-connected PV systems, positioning them as a promising avenue for advancing renewable energy technologies. However, the practical implementation of the proposed method is crucial for validating simulation results and identifying potential challenges in real-world applications. This aspect has been assigned as a focus for future studies of the present research.

The results demonstrate that building geometry, floor configuration, and block arrangement significantly influence both energy consumption and thermal comfort. High-rise buildings with fewer shared walls and larger exposed surfaces tend to exhibit higher heating and cooling loads, whereas designs incorporating shared walls and optimized block layouts reduce energy demand while maintaining occupant comfort. These findings underscore the importance of integrating energy-efficient design strategies with climate-responsive planning to achieve sustainable and comfortable residential developments across diverse urban contexts.

The results demonstrated that the number of shared walls has a more significant influence on energy performance than the number of floors. Specifically, single-story buildings without shared walls exhibited up to 58.9% higher heating loads and 67.1% higher cooling loads compared to scenarios with greater wall adjacency. On average, the difference in energy consumption between the buildings with the maximum and minimum number of common walls was approximately 60%. Moreover, heat loss through the roof of a one-story building was found to be nearly 30 times greater than that of high-rise buildings with multiple units (Figure 9).

Additionally, exterior façade simulations were performed and analyzed to further assess their impact on energy performance. Future research will focus on examining the potential of phase change materials in reducing energy consumption in both high-rise and low-rise buildings.

Nomenclature

G	Ambient irradiation (W/m^2)
I_{ph}	Photocurrent (A)
I_d	Diode reverse saturation current (A)
R_s	Series resistance
R_{sh}	Shunt resistance
N_S	The count of solar cells connected in series
N_P	The number of parallel-connected cell strings
q	Electron charge, $\sim 1.602 \times 10^{-19}\ C$
k	Boltzmann constant, $\sim 1.381 \times 10^{-23}\ J/K$
A	Ideality factor
V_{oc}	Open-circuit voltage
I_{SC}	Short-circuit current
T_C	Reference temperature
I_C	Reference saturation current
E_g	Band gap energy
P_{max}	Maximum power point
$I_{sc,Tc}$	Designate the short-circuit current measured at a specific reference temperature
$V_{oc,Tc}$	Designate the open-circuit voltage measured at a specific reference temperature
ΔT	Defined as $T - Tc$, quantifies the deviation between the current cell temperature (T), and the reference temperature (T_C)
K_i	The temperature coefficient that quantifies how the short-circuit current changes with temperature variations
S	Denotes the solar irradiation, expressed in mW/cm^2
P	Total output power of the PV array
η_{inst}	The steady-state efficiency
$P_{pv-meas}$	The actual power output produced by the solar panel
$P_{MPP-ideal}$	The theoretical maximum power that the solar panel is capable of generating under ideal conditions
$\eta_{dynamic}$	The dynamic efficiency
$V_{pv-meas}$	The actual output voltage produced by the solar panel
V_{MPP}	The theoretical maximum voltage that the solar panel is capable of generating under MPP conditions
y(k)	The output signal
u(k)	The input signal
$\varphi(k)$	The past and current input data
$\hat{\theta}(k)$	Estimated parameter vector
$\varepsilon(k)$	Prediction error
a_i, b_i	The coefficients that must be determined through estimation
$W_t(i)$	The PV module capacity validity coefficient
W_{batt}	The total power available from the battery pack when operating in discharge mode
$P_t(i)$	The effective load power
N_j	Number of consumers at load point j
λ_j	Average failure rate at load point j
U_j	Average annual outage time at load point j
$L_a(j)$	Average load connected to load point i

Appendix

For load points 37-47 the calculations of basic system indices are shown in table A_1.

Table A_1. Calculation of basic system indices for load points 37-47.

	Load point																							
	37		38		39		40		41		42		43		44		45		46		47			
Line	λ	r	λ	r	λ	r	λ	r	λ	r	λ	r	λ	r	λ	r	λ	r	λ	r	λ	r		
71	0.0485	4	0	0	0	0	0	0	0	0	0	0	0	0	0	0	0	0	0	0	0	0		
72	0.07125	0.4	0.07125	4	0.07125	1.61	0.07125	1.61	0.07125	1.61	0.07125	1.61	0.07125	1.61	0.07125	1.61	0.07125	1.61	0.07125	1.61	0.07125	1.61		
73	0	0	0.0485	4	0	0	0	0	0	0	0	0	0	0	0	0	0	0	0	0	0	0		
74	0.07125	0.4	0.07125	0.4	0.07125	4	0.07125	1.61	0.07125	1.61	0.07125	1.61	0.07125	1.61	0.07125	1.61	0.07125	1.61	0.07125	1.61	0.07125	1.61		
75	0	0	0	0	0.0485	4	0	0	0	0	0	0	0	0	0	0	0	0	0	0	0	0		
76	0.07125	0.4	0.07125	0.4	0.07125	0.4	0.07125	4	0.07125	1.61	0.07125	1.61	0.07125	1.61	0.07125	1.61	0.07125	1.61	0.07125	1.61	0.07125	1.61		
77	0	0	0	0	0	0	0.0485	4	0	0	0	0	0	0	0	0	0	0	0	0	0	0		
78	0.07125	0.4	0.07125	0.4	0.07215	0.4	0.07125	0.4	0.07125	4	0.07125	1.61	0.07125	1.61	0.07125	1.61	0.07125	1.61	0.07125	1.61	0.07125	1.61		
79	0	0	0	0	0	0	0	0	0.0485	4	0	0	0	0	0	0	0	0	0	0	0	0		
80	0.07125	0.4	0.07125	0.4	0.07125	0.4	0.07125	0.4	0.07125	0.4	0.07125	4	0.07125	1.61	0.07125	1.61	0.07125	1.61	0.07125	1.61	0.07125	1.61		
81	0	0	0	0	0	0	0	0	0	0	0.0485	4	0	0	0	0	0	0	0	0	0	0		
82	0.07125	0.4	0.07125	0.4	0.07125	0.4	0.07125	0.4	0.07125	0.4	0.07125	0.4	0.07125	4	0.07125	4	0.07125	4	0.07125	4	0.07125	4		
83	0	0	0	0	0	0	0	0	0	0	0	0	0.03395	4	0.03395	4	0.03395	4	0.03395	4	0.03395	4		
84	0	0	0	0	0	0	0	0	0	0	0	0	0.0388	4	0.0388	4	0.0388	4	0.0388	4	0.0388	4		
85	0	0	0	0	0	0	0	0	0	0	0	0	0	0	0.03395	4	0.03395	4	0.03395	4	0.03395	4		
86	0	0	0	0	0	0	0	0	0	0	0	0	0	0	0.0388	4	0.0388	4	0.0388	4	0.0388	4		
87	0	0	0	0	0	0	0	0	0	0	0	0	0	0	0.0388	4	0.0388	4	0.0388	4	0.0388	4		
88	0	0	0	0	0	0	0	0	0	0	0	0	0	0	0.0388	4	0.0388	4	0.0388	4	0.0388	4		
89	0	0	0	0	0	0	0	0	0	0	0	0	0	0	0.0388	4	0.0388	4	0.0388	4	0.0388	4		
90	0	0	0	0	0	0	0	0	0	0	0	0	0	0	0.0388	4	0.0388	4	0.0388	4	0.0388	4		
91	0	0	0	0	0	0	0	0	0	0	0	0	0	0	0.0388	4	0.0388	4	0.0388	4	0.0388	4		
	0.476	0.7668	0.476	1.3057	0.476	1.4868	0.476	1.6679	0.476	1.849	0.476	2.0301	0.50025	2.2979	0.767	2.8899	0.767	2.8899	0.767	2.8899	0.767	2.8899		
	U=0.365		U=0.6215		U=0.7077125		U=0.793925		U=0.880137		U=0.96635		U=1.14956		U=2.21656		U=2.21656		U=2.21656		U=2.21656			

References

[1] Q. Bi, G. Zhou, L. Deng, and N. Xue, "Target Voltage Iterations Based Global Flexible Power Point Tracking Algorithm Under Partial Shading Photovoltaic Systems," *IEEE Transactions on Sustainable Energy*, vol. 15, no. 1, pp. 236–248, 2024.

[2] B. Mandal, and P. S. Bhowmik, "A Deep Neural Network-Based Highly Simplified Intelligent Approach for Maximum Power Point Tracking of Dye-Sensitized Solar Panel System," *IEEE Journal of Emerging and Selected Topics in Industrial Electronics*, vol. 6, no. 1, pp. 196–203, 2025.

[3] A. Motovilov, and S. Lutchenko, "Calculation of Mean Time to Failure of Infocommunication System Wich Failure Rate Is Cycle Changed," *2022 Dynamics of Systems, Mechanisms and Machines (Dynamics)*, pp. 1–4, 2022.

[4] L. T. Ostrom and C. A. Wilhelmsen, “Probabilistic Risk Assessment,” in *Risk Assessment: Tools, Techniques, and their Applications*, John Wiley & Sons, ch. 15, pp. 223-230, 2012.

[5] H. E. Moumen, N. E. Akchioui, and A. Toukmati, "Continuous-Time Markov Processes for Reliability Analysis: A Comprehensive Study," *2024 4th International Conference on Innovative Research in Applied Science, Engineering and Technology (IRASET)*, pp. 1–8, 2024.

[6] I. Mehdi, E. M. Boudi, and M. A. Mehdi, "Reliability, Availability, and Maintainability Assessment of a Mechatronic System Based on Timed Colored Petri Nets," *Applied Sciences*, vol. 14, no. 11, 4852, 2024.

[7] M. Čepin, "Reliability Block Diagram," *Assessment of Power System Reliability*, pp. 119–123, 2011.

[8] A. Reza Reisi, M. Hassan Moradi, and S. Jamasb, "Classification and Comparison of Maximum Power Point Tracking Techniques for Photovoltaic System: A Review," *Renewable and Sustainable Energy Reviews*, vol. 19, pp. 433–443, 2013.

[9] Z. Chen, X. Sun, et al., "Maximum Efficiency Tracking Control for Omnidirectional Wireless Power Transfer System Based on AdamW Algorithm," *IEEE Transactions on Power Electronics*, vol. 40, no. 3, pp. 4602–4612, 2025.

[10] M. A. G. de Brito, L. Galotto, L. P. Sampaio, G. d. A. e Melo, and C. A. Canesin, "Evaluation of the Main MPPT Techniques for Photovoltaic Applications," *IEEE Transactions on Industrial Electronics*, vol. 60, no. 3, pp. 1156–1167, 2013.

[11] M. H. Moradi, and A. R. Reisi, "A Hybrid Maximum Power Point Tracking Method for Photovoltaic Systems," *Solar Energy*, vol. 85, no. 11, pp. 2965–2976, 2011.

[12] J. Jiang, Y. Su, et al., "On Application of a New Hybrid Maximum Power Point Tracking (MPPT) Based Photovoltaic System to the Closed Plant Factory," *Applied Energy*, vol. 124, pp. 309–324, 2014.

[13] H. Park, and H. Kim, "PV Cell Modeling on Single-Diode Equivalent Circuit," *IECON 2013 - 39th Annual Conference of the IEEE Industrial Electronics Society*, pp. 1845–1849, 2013.

[14] N. M. A. Alrahim Shannan, N. Z. Yahaya, and B. Singh, "Single-Diode Model and Two-Diode Model of PV Modules: A Comparison," *2013 IEEE International Conference on Control System, Computing and Engineering*, pp. 210–214, 2013.

[15] A. Sakhare, and S. Mikkili, "Enhancing Photovoltaic Array Performance Through the Integration of Perturb and Observe MPPT and Novel Ladder Configuration," *e-Prime - Advances in Electrical Engineering, Electronics and Energy*, vol. 11, 100943, 2025.

[16] D. Sharma, M. F. Jalil, M. S. Ansari, and R. C. Bansal, "A Review of Maximum Power Point Tracking (MPPT) Techniques for Photovoltaic Array Under Mismatch Conditions," *Photovoltaic Systems Technology*, pp. 85–102, 2024.

[17] S. Hassan Hakmi, H. Alnami, A. Ginidi, A. Shaheen, and T. A. Alghamdi, "A Fractional Order-Kepler Optimization Algorithm (FO-KOA) for Single and Double-Diode Parameters PV Cell Extraction," *Heliyon*, vol. 10, no. 16, e35771, 2024.

[18] A. O. Salau, S. K. Maitra, A. Kumar, A. Mane, and R. W. Dumicho, "Design, Modeling, and Simulation of a PV/Diesel/Battery Hybrid Energy System for an Off-Grid Hospital in Ethiopia," *e-Prime - Advances in Electrical Engineering, Electronics and Energy*, vol. 8, 100607, 2024.

[19] K. Ishaque, Z. Salam, and H. Taheri, "Simple, Fast and Accurate Two-Diode Model for Photovoltaic Modules," *Solar Energy Materials and Solar Cells*, vol. 95, no. 2, pp. 586–594, 2011.

[20] I. H. Altas, and A. Sharaf, "A Photovoltaic Array Simulation Model for Matlab-Simulink GUI Environment," *2007 International Conference on Clean Electrical Power*, pp. 341–345, 2007.

[21] G. Singh, "Solar Power Generation by PV (photovoltaic) Technology: A Review," *Energy*, vol. 53, pp. 1–13, 2013.

[22] H. Patel, and V. Agarwal, "MATLAB-Based Modeling to Study the Effects of Partial Shading on PV Array Characteristics," *IEEE Transactions on Energy Conversion*, vol. 23, no. 1, pp. 302–310, 2008.

[23] K. Ishaque, Z. Salam, H. Taheri, and Syafaruddin, "Modeling and Simulation of Photovoltaic (PV) System During Partial Shading Based on a Two-Diode Model," *Simulation Modelling Practice and Theory*, vol. 19, no. 7, pp. 1613–1626, 2011.

[24] N. A. Meineri, I. Santana, and I. G. Zurbriggen, "Ultra-Fast MPPT for Residential PV Systems with Low DC-Link Capacitance and Differential Power Processing," *IEEE Transactions on Power Electronics*, vol. 40, no. 2, pp. 2736–2745, 2025.

[25] D. Sera, T. Kerekes, R. Teodorescu, and F. Blaabjerg, "Improved MPPT Algorithms for Rapidly Changing Environmental Conditions," *2006 12th International Power Electronics and Motion Control Conference*, pp. 1614–1619, 2006.

[26] W. Marańda and M. Piotrowicz, "Static and Dynamic MPP-Tracking Efficiency of PV-Inverter Using Recorded Irradiance," *International Journal of Microelectronics and Computer Science*, vol. 4, no. 4, pp. 181–185, 2013.

[27] V. Bobál, J. Böhm, J. Fessl, and J. Macháček, *Digital self-tuning controllers: algorithms, implementation and applications*. London: Springer London, 2005.

[28] H. Qiang, S. Qiao, H. Huang, P. Cheng, and Y. Sun, "Nonlinear Adaptive Control of Maglev System Based on Parameter Identification," *Actuators*, vol. 14, no. 3, 115, 2025.

[29] R. N. Allan, *Reliability Evaluation of Power Systems*. Springer Science & Business Media, 2013.

[30] T. Esram, and P. L. Chapman, "Comparison of Photovoltaic Array Maximum Power Point Tracking Techniques," *IEEE Transactions on Energy Conversion*, vol. 22, no. 2, pp. 439–449, 2007.

[31] N. Kasa, T. Iida, and L. Chen, "Flyback Inverter Controlled by Sensorless Current MPPT for Photovoltaic Power System," *IEEE Transactions on Industrial Electronics*, vol. 52, no. 4, pp. 1145–1152, 2005.

Declaration of competing interest

The authors declare that they have no known competing financial interests or personal relationships that could have appeared to influence the work reported in this paper. The ethical issues, including plagiarism, informed consent, misconduct, data fabrication and/or falsification, double publication and/or submission, redundancy, have been completely observed by the authors.

Bibliography

Peyman Bayat received the bachelor's and master's degrees from Hamedan University of Technology and Bu-Ali Sina University, respectively, and the Ph.D. degree from University of Guilan. Since 2018, he has been with Hamadan University of Technology, where he is currently an Assistant Professor in electrical engineering. His research area includes microgrids, power electronics, electric vehicles, smart grids, sustainable energy, artificial intelligence etc. He is a reviewer of several IEEE and Elsevier journals, such as sustainable cities and society, applied energy, energy storage and many others.
Email: peyman.bayat@hut.ac.ir
ORCID: 0000-0001-7289-825X
Contribution Statement: Conceptualization, Data curation, Formal analysis, Funding acquisition, Investigation, Methodology, Project administration, Resources, Software, Supervision, Validation, Visualization, Roles/Writing - original draft, Writing-review & editing.

Pezhman Bayat is currently working as an Assistant Professor (7 + Years Exp.) in the Department of Electrical Engineering at Hamedan University of Technology. He has completed his Ph.D. from University of Guilan. He has over 12 years research experience in power electronics, machines and drives. His research interests include electric vehicles, renewable energy systems, power electronics etc. He has published over 30 papers and supervised over 20 students to completion. Dr. Bayat is a reviewer of several journals, such as Elsevier journals, IEEE transactions on power electronics, IEEE transactions on industrial electronics, Taylor & Francis international Journal of Electronics, and many others.
Email: pezhman.bayat@hut.ac.ir
ORCID: 0000-0003-0598-841X
Contribution Statement: Conceptualization, Data curation, Formal analysis, Funding acquisition, Investigation, Methodology, Project administration, Resources, Software, Supervision, Validation, Visualization, Roles/Writing-original draft, Writing-review & editing.